CHEMMEDCHEM

DOI: 10.1002/cmdc.200800025

Isoquinolin-1-one Inhibitors of the MDM2–p53 Interaction

Ulli Rothweiler,[b] Anna Czarna,[b] Marcin Krajewski,[b] Jolanta Ciombor,[b] Cédric Kalinski,[c] Vladimir Khazak,[a] Günther Ross,[c] Natalia Skobeleva,[d] Lutz Weber,*[a] and Tad A. Holak*[b]

p53 has been at the centre of attention for drug design since the discovery of its growth-suppressive and pro-apoptotic activity. Herein we report the design and characterisation of a new class of isoquinolinone inhibitors of the MDM2–p53 interaction. Our identification of druglike and selective inhibitors of this protein–protein interaction included a straightforward in silico compound-selection process, a recently reported NMR spectroscopic approach for studying the MDM2–p53 interaction, and selectivity screening assays using cells with the same genetic background. The selected inhibitors were all able to induce apoptosis and the expression of p53-related genes, but only the isoquinolin-1-one-based inhibitors stabilised p53. Our NMR experiments give a persuading explanation for these results, showing that isoquinolin-1-one derivates are able to dissociate the preformed MDM2–p53 complex in vitro, releasing a folded and soluble p53. The joint application of these methods provides a framework for the discovery of protein interaction inhibitors as a promising starting point for further drug design.

Introduction

The human p53 tumour suppressor protein has been one of the most investigated proteins in cancer research due to the fact that loss of p53 function through mutation and/or deregulation is involved in more than 50% of all human cancers. The role of p53 in controlling the cell cycle and monitoring the integrity of the genome has made it known as the "guardian of the genome".[1] p53 is activated by a number of genotoxic factors such as ionising radiation and cytotoxic compounds.[2] Subsequent stabilisation by posttranslational mechanisms, accumulation, and translocation of p53 to the nucleus and mitochondria leads to the activation of proteins involved in cell-cycle arrest, DNA repair, and apoptosis. p53 is tightly controlled in the non-stressed cell by its cellular antagonist MDM2 (murine double minute 2) through an autoregulatory feedback loop,[3] that is, MDM2 is transcriptionally activated by p53, which can in turn block the function of p53 by several mechanisms. First, MDM2 binds to the N-terminal transactivation domain of p53, resulting in an inhibition of p53-mediated transactivation. Second, MDM2 has a nuclear export signal, and shuttles the MDM2–p53 complex out of the nucleus into the cytosol. There it serves as a ubiquitin ligase and targets p53 for degradation through the proteasome pathway.[4] Besides the functional loss of p53 through mutation, it can also be inactivated by the overexpression or amplification of MDM2, which is the case in many tumours.[5] Several studies have shown that the disruption of the MDM2–p53 interaction or suppression of MDM2 expression can activate the p53 pathway and inhibit tumour growth.[6] Thus, disruption of the MDM2–p53 interaction is considered a novel therapeutic strategy for cancer cells that still are endowed with wild-type p53,[7] and a variety of small-molecule druglike compounds have been reported that bind at the p53 binding site of MDM2 (compounds **1**, **2**, and **3**, Figure 1).[8]

The discovery of small molecules that inhibit protein–protein interactions remains a challenge, although significant progress

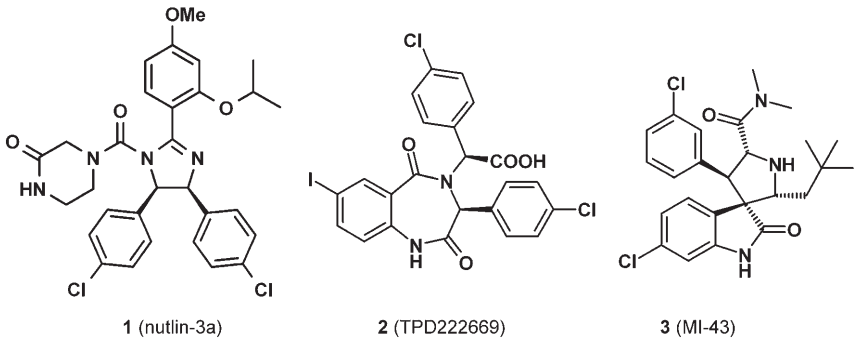

1 (nutlin-3a) **2** (TPD222669) **3** (MI-43)

Figure 1. Published MDM2–p53 inhibitors **1**, **2**, and **3**.

[a] *Dr. V. Khazak, Dr. L. Weber*
NexusPharma Inc., #253-13 Summit Square Center
Langhorne, PA 19047-1098 (USA)
Fax: (+1) 215-214-1622
E-mail: lutz.weber@nexuspharm.com

[b] *Dr. U. Rothweiler, A. Czarna, Dr. M. Krajewski, J. Ciombor, Dr. T. A. Holak*
Max Planck Institute for Biochemistry, 82152 Martinsried (Germany)
Fax: (+49) 89-8578-3777
E-mail: holak@biochem.mpg.de

[c] *Dr. C. Kalinski, Dr. G. Ross*
Priaxon AG, Gmunder Str. 37–37a, 81379 München (Germany)

[d] *Dr. N. Skobeleva*
Fox Chase Cancer Center, Philadelphia, PA 19111 (USA)

has been made over the last few years.[9] Traditional cell-free protein-based high-throughput screening approaches or in silico compound screening have often yielded rather hydrophobic molecules that are promiscuous binders and may act through "unfriendly" binding and unfolding of the interacting proteins.[10] Methods are therefore needed that are not only able to propose useful molecules, but also to rapidly identify and discard false-positive screening hits. Ideally, we propose the use of orthogonal biophysical and cellular assays in parallel to identify useful and robust starting points for a potential medicinal chemistry program.

We recently described an NMR method that allows direct monitoring of the influence of a ligand on protein–protein binding.[11,12] This method uses chemical shift perturbations in 2D ^{1}H–^{15}N heteronuclear single-quantum coherence (HSQC) spectra of ^{15}N-labelled proteins to monitor the inhibitors' influence on protein–protein interactions.[11]

The size of the ^{15}N-labelled reporter protein should be small enough to give a good-quality HSQC spectrum. When a larger unlabelled protein binds to the smaller one, the observed $1/t_2$ transverse relaxation time of the bound reporter protein in the complex increases, resulting in broadening of NMR resonances and consequently disappearance of the signals in the HSQC spectrum. An antagonist that competes for the same binding site with the protein would be able to completely or partially restore the ^{15}N HSQC spectrum. Weak inhibitors would be unable to restore the ^{15}N HSQC spectrum or able to do so only when added in large excess. This method also permits determinations of whether a small molecule is capable of releasing proteins in their wild-type folded states or whether it induces their denaturation, partial unfolding, or precipitation.[11,12]

Results and Discussion

Design and synthesis

The knowledge of structurally diverse ligands such as **1**–**3** provides a good basis for ligand-based scaffold-hopping compound selection and design. For this purpose, we collected about seven million compounds from commercial vendors as a starting point. Screening for structurally similar compounds with alternative scaffolds ("scaffold hopping") was performed by using a modified topological torsion (TT) substructure descriptor,[13] which has the form:

$$M\ ACHP_i\ ACHP_j\ ACHP_k\ ACHP_l$$

for which i, j, k, and l are consecutively bonded atoms, *M* is the multiplicity of a given unique TT found in the compound, *A* is the atom number, *C* is the charge, *H* is the number of attached hydrogen atoms, and *P* is the number of π electrons on the respective atom. Our descriptor differs from other recent implementations[14] by the use of *M* and that the number of possible atom types is not limited by predefined conventions. This atom pair descriptor method[15] delivers structurally similar compounds, but neglects the concept of core scaffolds that are implicitly or explicitly encoded in many other typical 2D similarity search methods. Nutlin-3 (**1**) was then used as a probe to extract similar compounds from our vendors' database. Whereas conventional similarity screening implemented in chemical databases yields, as expected, imidazoline-type compounds as most similar, our TT-based 2D similarity screening delivered 278 similar compounds of various scaffolds. Using the program LIGSITE^{csc},[16] the p53 binding site of MDM2 was extracted from the X-ray crystal structure (PDB code: 1RV1, Figure 2), and after generating a library of conformers, molecules from the 2D selection step were further evaluated for their 3D shape fit with the p53 binding pocket.

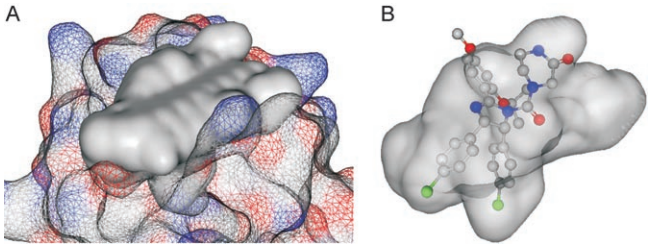

Figure 2. A) MDM2 (mesh, atom type) and binding pocket (generated with LIGSITE^{csc}, solid surface); B) extracted MDM2 pocket (transparent) superimposed with **1** based on the crystal structure (PDB code: 1RV1).

The respective shape similarities were calculated using the program M3dsml from the Moloc program package.[17] As a result, a prioritised list of 131 compounds was obtained with **1** as an initial seed for ligand-based design: on ranks 1 and 2, two benzodiazepines (**4** and **5**) are found as most similar, rank 3 is an imidazoline **6**, rank 4 is an isoquinolin-1-one **7**, and rank 5 is a pyrrolin-2-one **8** (Figure 3).

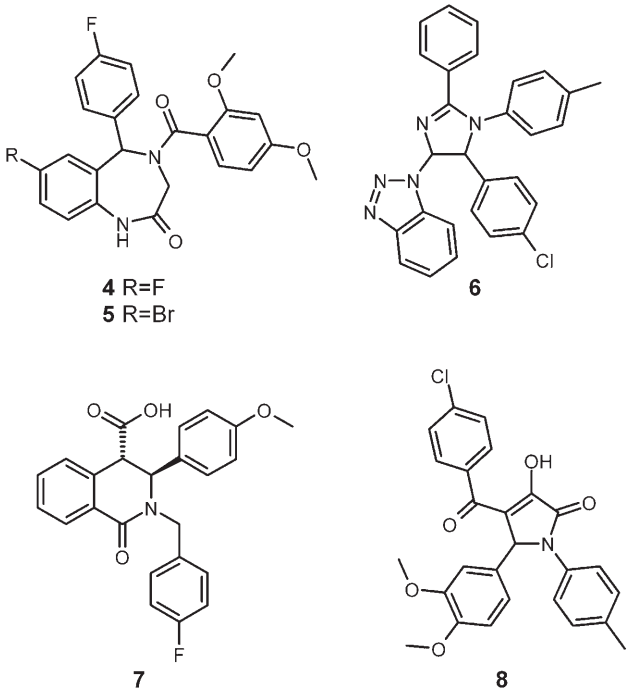

Figure 3. MDM2 binding pocket and top-ranking in silico screening hits **4**–**8** from a library of commercially available compounds.

Compounds **7** and **8** represent novel scaffolds for potential MDM2–p53 interaction inhibitors. Based on these proposals we first synthesised NXN-6, NXN-7, and NXN-11, considering that the MDM2 pocket has a preference for two chloro-substituted phenyl substituents (Schemes 1 and 2). The respective tetrahydroisoquinolin-1-one-4-carboxylic acids as analogues of **7** can be obtained in a one-pot reaction by using homophthalic acid, an aromatic aldehyde, and a primary amine.[18] Usually, the thermodynamically more stable *trans* product is prepared by treating the mixture of isomers in acetic acid at reflux.[18b] In the recent past, different methods were developed to synthesise pure isomers. The use of Lewis acid catalysts such as boron trifluoride diethyl ether ($BF_3{\cdot}Et_2O$) allows direct formation of *trans*-isoquinolinic acid derivatives.[18d] On the other hand, ionic liquids have been employed for the synthesis of *cis* isomers.[18e] Subsequent amide formation with the free carboxylic acid is straightforward and best performed by aminolysis of a pentafluorophenyl ester (Scheme 1) or coupling of the acid and an amine with a peptide-coupling agent. X-ray crystallographic analysis of related compounds has shown previously that the substituents at positions 3 and 4 adopt a bis-pseudoaxial conformation,[19] which is in agreement with the desired conformation for the best overlap with the p53 binding pocket.

Compounds NXN-552, -553, and -561 were synthesised as more advanced analogues to mimic the tryptophan residue of p53 in the MDM2 binding site, while the piperazine group of NXN-561 should increase the solubility of this compound series. Similarly, the pyrrolin-2-one NXN-11 was synthesised as a readily available analogue of **8** in a one-pot reaction from 2-oxo-3-phenylpropionic acid, 4-chlorobenzaldehyde, and 4-chlorobenzylamine (Scheme 2).

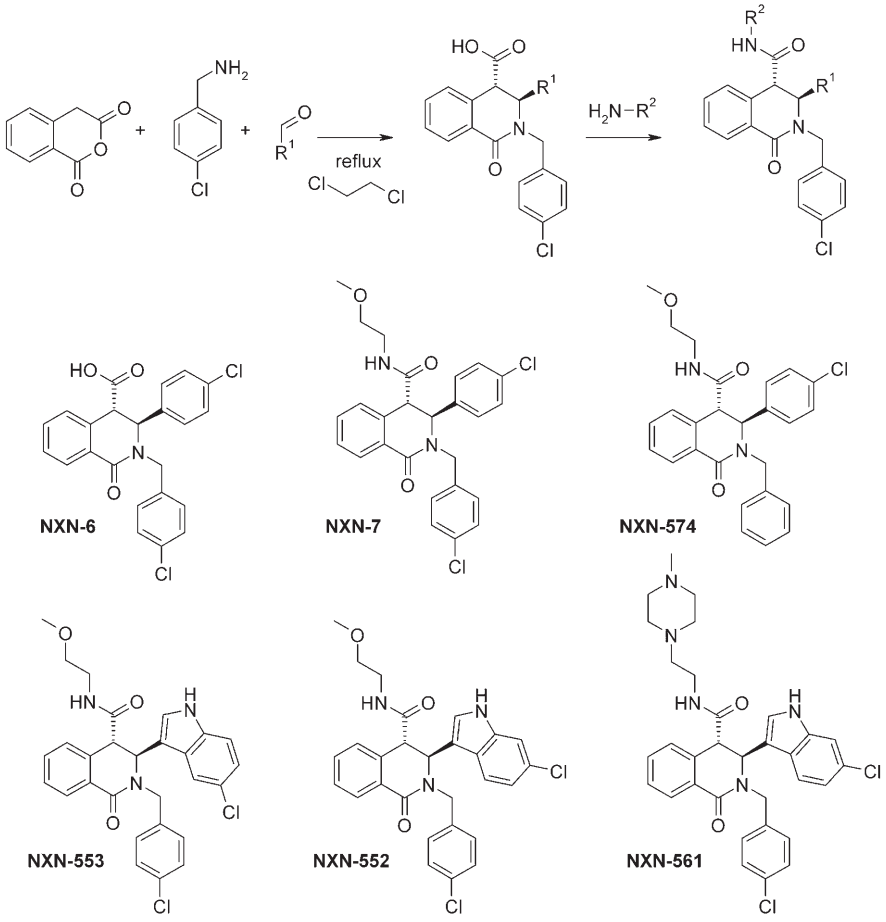

Scheme 1. Synthesis of NXN-6, NXN-7, NXN-552, -553, -561, and -574 through a one-pot condensation reaction of a Schiff base with homophthalic acid followed by amide bond formation.

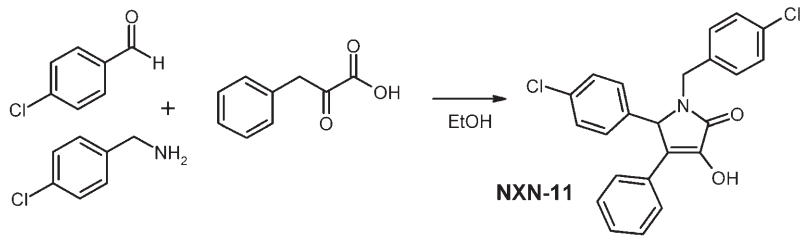

Scheme 2. Synthesis of NXN-11 through a one-pot Doebner condensation of a Schiff base with α-keto acids.

Interaction with MDM2 (residues 1–118)

The novel compounds were tested for binding to MDM2 by performing a series of NMR titrations with isotopically enriched [^{15}N]MDM2.[11,20] Strong binding of a compound to its target is indicated by peak splitting in the HSQC spectrum, whereas a shift of peaks indicates weaker binding. Figure 4 shows ^{15}N HSQC spectra of MDM2 titrated with NXN-6. Approximately 25 residues of MDM2 are affected upon NXN-6 binding, but the spectra show a shift of peaks rather than splitting, which indicates that NXN-6 binds to MDM2 in rapid exchange. From the ^{15}N HSQC spectra we calculated a K_D^{NMR} value for NXN-6 of approximately 8 ± 4 μM. Similar results were obtained with NXN-7, with $K_D^{NMR} \sim 5$ μM, still a weakly binding inhibitor, but with slightly higher affinity than NXN-6 in binary NMR titrations.

As in the case of NXN-6, around 25 residues are affected upon binding of NXN-7 to

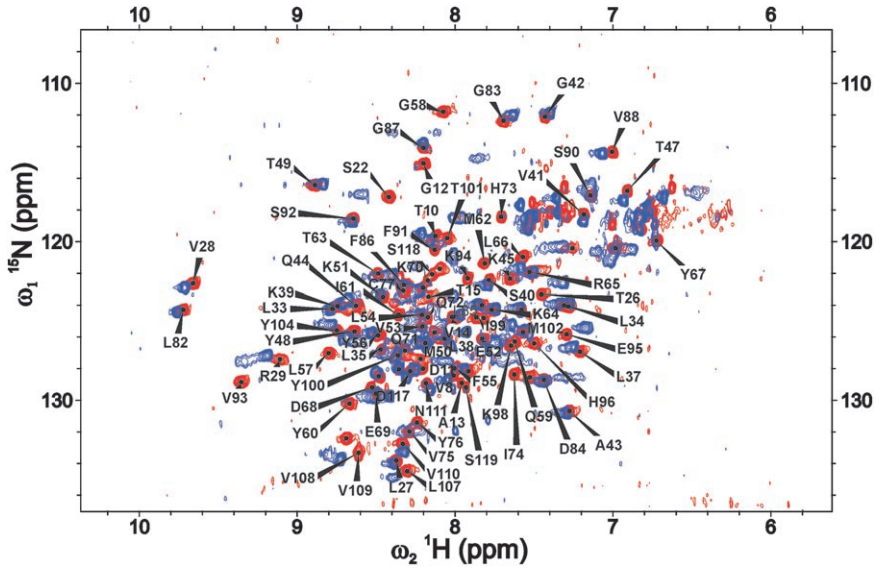

Figure 4. The MDM2 spectrum (red), and MDM2 + NXN-6 (blue); final concentration ratio of MDM2/NXN-6 = 1:10.

MDM2. The stronger binding of NXN-7 comes at the expense of decreased solubility. A surface plot of MDM2 bound to NXN-6 and NXN-7 shows that upon binding, the same residues of MDM2 and hence the binding region are affected in comparison with nutlin-3 binding, which is also the region involved in the binding of the p53 peptide (Figure 5).[17]

The structurally different third compound, NXN-11, binds only weakly to [^{15}N]MDM2, and only a few MDM2 residues are affected upon binding, indicating that there is only weak and more unspecific interaction between NXN-11 and MDM2. As observed in the surface plot of NXN-11, only few interacting residues are highlighted in dark (Figure 5C).

The structure–activity relationship of the new isoquinolone scaffold is similar to nutlin-3 and is highly dependent on the presence of two correctly positioned chloro-substituted aromatic rings in the inhibitors.[8,9,20] Thus, removal of a chloro group (in NXN-574), a shift by one position (in NXN-553), or replacement with other substituents such naphthalines or aliphatic side chains (compounds not shown) leads to inactive compounds.

The improved NXN compound NXN-561 was separated into its enantiomers in hopes of identifying the enantiomer that exhibits more specific cellular effects. Both enantiomers were tested separately for binding to MDM2, and surprisingly both enantiomers bind with almost the same K_D value as determined in isothermal titration calorimetry (ITC) and NMR experiments. Despite the fact that the binding K_D^{NMR} values for both enantiomers are similar, binding of the two enantiomers affect different residues on MDM2, as shown in Figure 6. Both enantiomers have the largest chemical shift on amino acids close to the binding pocket. (−)-NXN-561a shows the largest movements on residues T26, E52, F55, Y67, D68, H73, Y76, V93, K94, and E95. In contrast, (+)-NXN-561b affects primarily residues T26, L54, Y60, D68, H73, I74, V93, K98, and T101.

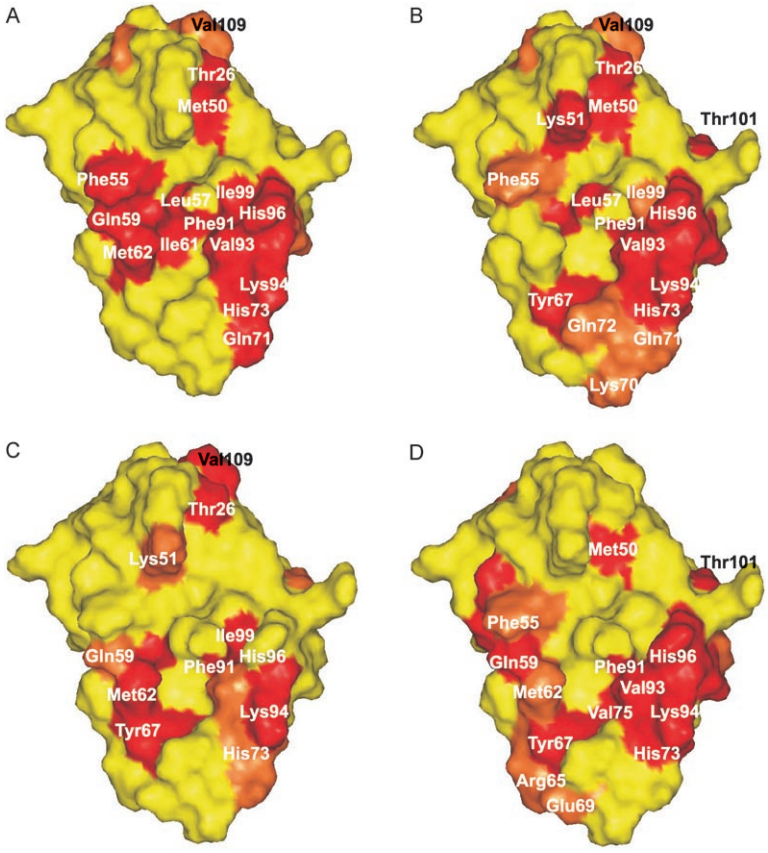

Figure 5. NXN effects on the surface of MDM2 observed by NMR titration. Red: NMR chemical shifts > 0.15 ppm or peaks are missing after addition of the compound; orange: shifts between 0.1 and 0.15 ppm; yellow: shifts < 0.1 or no shifts. A) NXN-6, B) NXN-7, C) NXN-11, D) nutlin-3.

Interaction with the MDM2$_{1-118}$–(GST-p53)$_{1-73}$ complex

Based on the results of the ^{15}N HSQC experiments, we performed a set of NMR experiments using the preformed MDM2–p53 complex to test whether NXN compounds are able to disrupt the interaction between these two proteins. Isotopically enriched [^{15}N]MDM2 was titrated against unlabelled glutathione-*S*-transferase–p53 fusion protein (GST-p53, residues 1–73). The disappearance of most of the MDM2 peaks due to a decrease in the transversal relaxation rate of the larger complex indicated formation of the complex. The

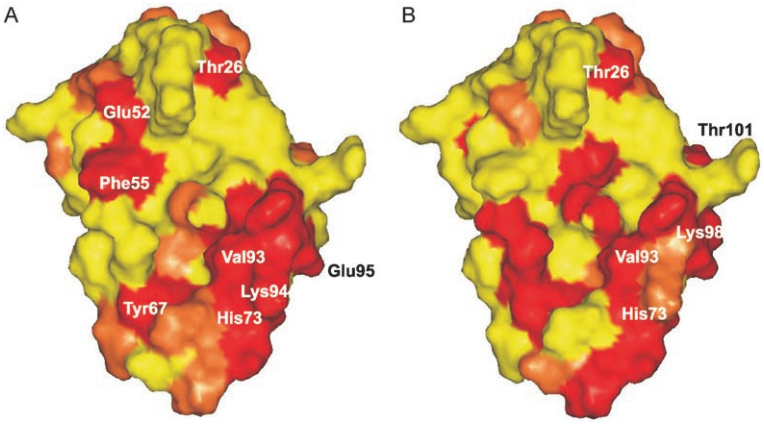

Figure 6. NXN-561 enantiomer effects on the surface of MDM2 observed by NMR titration. Red: NMR chemical shifts >0.15 ppm or peaks are missing after addition of the compound; orange: shifts between 0.1 and 0.15 ppm; yellow: shifts <0.1 or no shifts. A) NXN-561a, B) NXN-561b.

second step was the titration of the NXN compounds to this MDM2–GST-p53 complex, an assay we refer to as AIDA NMR.[11,12]

As shown in Figure 7, NXN-6 is able to dissociate and recover free MDM2 at an inhibitor/MDM2 ratio of 10:1. This recovery was indicated by the reappearance of the peaks in the [^{15}N]MDM2 HSQC spectrum, showing the dissociation of the complex. From the tryptophan side chain signal of p53 in the 1D NMR spectrum, we could estimate p53 recovery semi-quantitatively upon binding of NXN-6 and NXN-7 to the MDM2–GST-p53 complex (Figure 8, a 1D version of the AIDA NMR assay).

In contrast to the isoquinolinones, the pyrrolinone NXN-11 was unable to form a stable complex with MDM2, even with the inhibitor present in significant excess. The signals of all inhibitors were observed in the 1D NMR spectrum, showing that they were in excess in the final titration step. From the 1D spectra in Figure 8 we conclude that NXN-6 is the most effective compound under NMR conditions, with a recovery of GST-p53 of around 70%. NXN-7 and the two enantiomers of NXN-561 gave recovery rates from 60 to 70%, being only slightly less effective. Because all binding K_D^{NMR} values are quite similar, similar recovery rates are expected. The observed variations might result from the differences in compound solubility.

Isothermal titration calorimetry and Biacore experiments

In the isothermal titration calorimetry experiments we could clearly find binding of nutlin-3, the p53 peptide, and NXN-6 to the MDM2 protein independent of the presence of a co-solvent. In the case of NXN-6 it was shown that the nutlin-3 binding is significantly affected as well. For the other compounds the picture was not as clear: NXN-7 and NXN-552 showed binding to the protein under standard conditions and in competition with nutlin-3, but when the co-solvent Brij was added, no significant signal could be obtained (the selection of detergent may induce secondary effects on binding, for example, interaction with hydrophobic binding interface and competition).

The contribution of ΔH to ΔG was 3–10-fold higher than $T\Delta S$ in all reactions, which makes these reactions enthalpically driven. Akin to the NMR experiments, NXN-11 showed indifferent results (Table 1).

Similar results were also obtained in Biacore experiments. A clear binding of nutlin-3, the p53 peptide, and the compounds NXN-6 and NXN-7 was observed, and the respective $K_D^{Biacore}$ values were determined. Again, nutlin-3 and NXN-6 displayed binding competition with the p53 peptide and 1:1 complex formation. The binding kinetics showed very fast on- and off-rate kinetics. For NXN-7 and even more pronounced with NXN-552, the binding decreased at higher concentrations because of the lower solubility of the compounds. NXN-11 did not show any binding in Biacore experiments, in agreement with the ITC and NMR data.

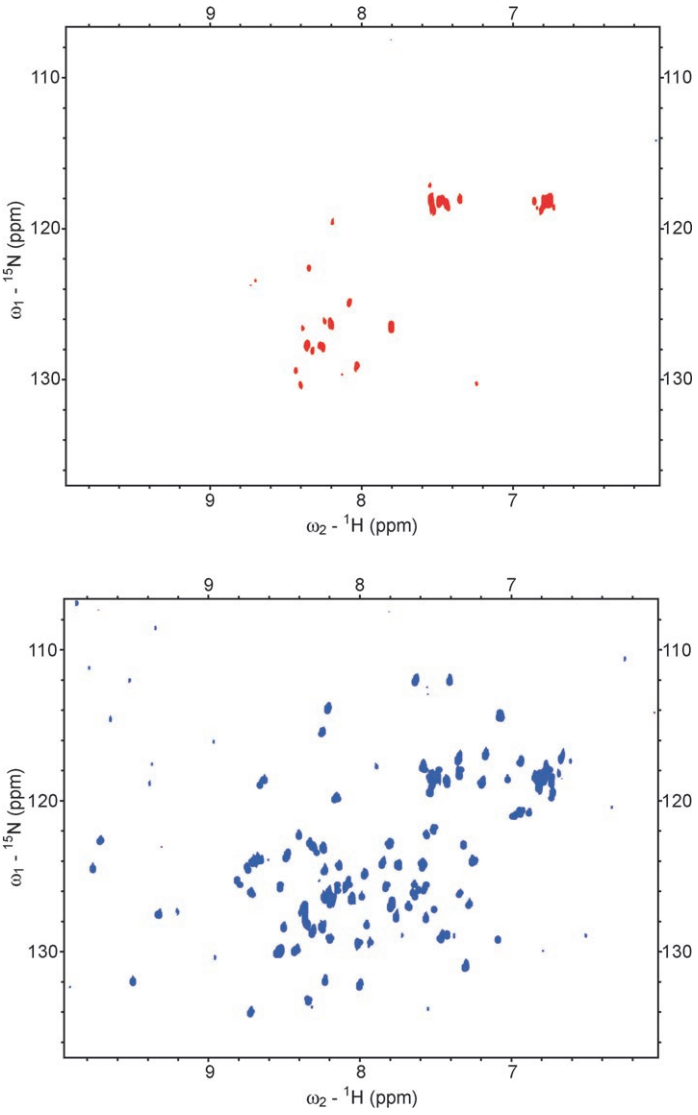

Figure 7. ^{1}H–^{15}N HSQC titration with the MDM2–GST-p53 (res. 1–73) complex and NXN-6. Complex formation is observed in the upper spectrum, and most of the cross-peaks had disappeared; only flexible residues are visible. The MDM2 spectrum is restored after addition of NXN-6 (lower spectrum).[11]

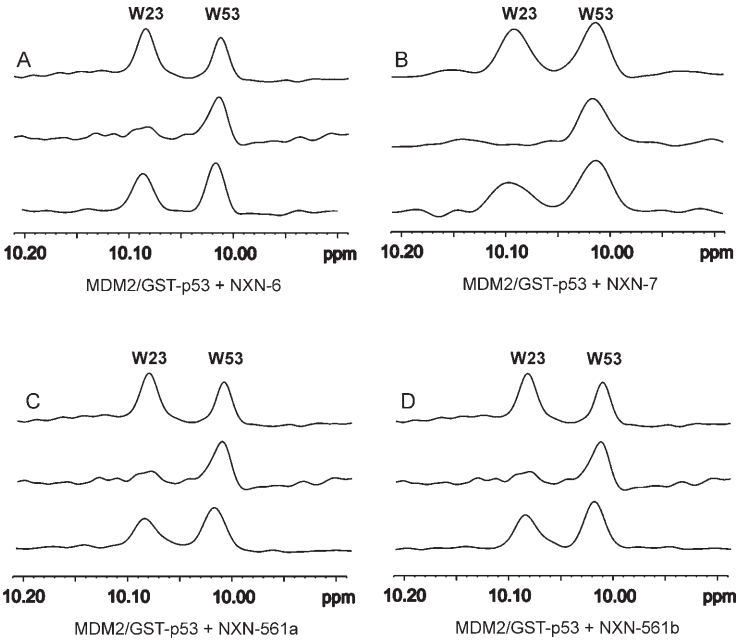

Figure 8. 1D AIDA with NXN compounds. Upper trace: spectrum of GST-p53 (res. 1–73). The two peaks are tryptophan residues W23 and W53. Middle trace: spectrum of complex of GST-p53 (res. 1–73) + MDM2 (res. 1–118). Tryptophan W23 is in the binding site and therefore disappears on binding to MDM2. Lower trace: Addition of NXN compounds to the complex releases GST-p53 as observed by the reappearance of tryptophan W23. A) NXN-6,[21] B) NXN-7, C) NXN-561a, D) NXN-561b. NXN-7 was recorded at 500 MHz, and the other three were recorded at 600 MHz.

Table 1. Binding affinity and cellular activity of compounds [μM].

Compound	K_D^{NMR}	K_D^{ITC}	$K_D^{Biacore}$	PA-1	PA-1/E6
NXN-6	8[a]; 2[b]	2	21	>60	>60
NXN-7	5[a]; 4[b]	4.0	11	27.1	62.5
NXN-11	>200[a]	no fit	no fit	12.2	26.2
NXN-552	n.d.	5.0	no fit	23.0	>60
NXN-561a	5[a]; 2[b]	2.5	n.d.[c]	6.3	11.5
NXN-561b	5[a]; 2[b]	2.0	n.d.[c]	9.0	12.2
nutlin-3	<1	0.7[22]	0.045	4.6	>60

[a] K_D calculated from binary titration.[20] [b] K_D calculated from the AIDA recovery experiment.[12] [c] Not determined.

Proliferation assays

The NXN compounds were tested for their ability to modulate viability and proliferation of the PA-1 ovarian teratocarcinoma cell line, which expresses the wild-type form of p53 and a PA-1/E6 cell line, which was stably transfected with the human papilloma virus HPV E6 gene, resulting in a dominant negative expression of p53.

Nutlin-3 was used as a positive control, decreasing the proliferation of PA-1 cells with an IC_{50} value of 4.6 μM (Table 1), whereas no effect on PA-1/E6 cells was observed in the concentration range tested. As expected, the PA-1 cells with wild-type p53 were more sensitive to treatment with NXN-7 and NXN-11, with IC_{50} values of 27.1 and 12.2 μM, respectively. Although NXN-7 and NXN-11 exhibited some antiproliferative effect in PA-1/E6 cells, the IC_{50} values for NXN-7 and NXN-11 were significantly higher than in the PA-1 cell line: 62.5 and 26.2 μM, respectively. NXN-6 did not show any activity in the cell lines; its free carboxylic acid most likely prevents entry into cells. The chemically more advanced analogue of NXN-7, NXN-561a, showed more effective inhibition of PA-1 cells with $IC_{50} = 6.3$ μM, but at the expense of selectivity over PA-1/E6 relative to NXN-552.

Analysis of apoptosis induction by NXN-7 and NXN-11

To test whether inhibition of PA-1 proliferation was associated with induction of apoptosis, we analysed the level of apoptosis in PA-1 and PA-1/E6 cells treated with NXN-7, NXN-11, and nutlin-3 using the Guava TUNEL and Guava annexin V assays. As shown in Figure 9, treatment of PA-1 cells with NXN-7 and NXN-11 for 48 h produced dose-dependent induction of apoptosis, represented by an increase in the number of TUNEL-positive cells. Interestingly, the number of positive apoptotic cells in samples treated with 40 μM NXN-7 and 20 μM NXN-11 were significantly higher than after treatment with 10 μM nutlin-3. However, both NXN-7 and NXN-11 caused a modest dose-dependent increase in the number of apoptotic cells in the PA-1/E6 cell line as well.

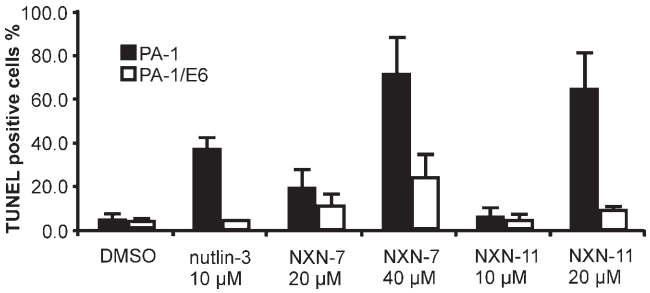

Figure 9. Guava TUNEL apoptosis assay with NXN-7, NXN-11, and nutlin-3 after 48 h treatment.

To further characterise apoptosis induction, we applied annexin V staining to PA-1 and PA-1/E6 cells treated for 48 h with NXN-7 and NXN-11, again using nutlin-3 as a positive control (Figure 10). Here, the number of annexin-V-positive PA-1 cells were similar in samples treated with nutlin-3 at 10 μM, NXN-7 at 40 μM, and NXN-11 at 20 μM, indicating that the NXN compounds trigger both late and early apoptosis events. The annexin V assay also revealed a modest increase of annexin-V-positive cells in PA-1/E6 samples treated with NXN-7, most likely through the interaction with an additional but unknown cellular protein.

The induction of apoptosis is frequently associated with proteolytic cleavage of specific apoptosis biomarkers, caspase-3 and poly(ADP-ribose) polymerase (PARP). To verify whether such cleavage occurred in PA-1 cells treated with the NXN

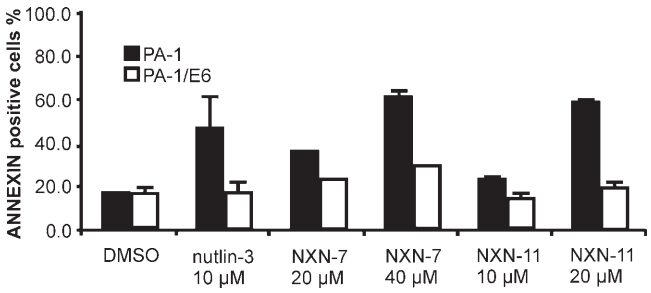

Figure 10. Guava annexin V apoptosis assay with NXN-7, NXN-11, and nutlin-3 after 48 h treatment.

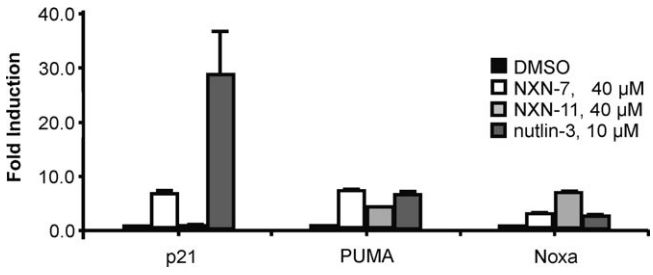

Figure 12. Induction of p53-regulated reporter genes p21, PUMA, and Noxa in PA-1 cells treated for 4 h with NXN compounds or nutlin-3.

compounds for 24 h, whole-protein extracts from these cells were subjected to Western blot analysis with monoclonal antibodies against cleaved caspase-3 and PARP. As shown in Figure 11, NXN-7 and NXN-11 were able to induce the proteolytic activation of caspase-3 and PARP degradation in a dose-dependent manner.

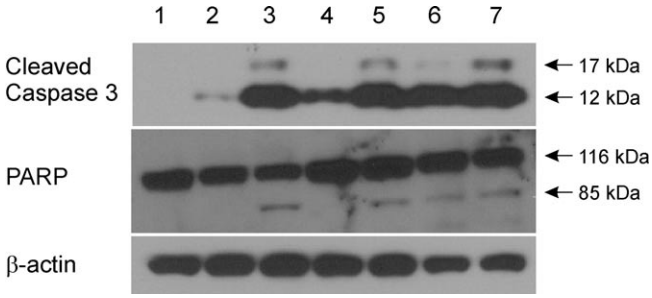

Figure 11. Induction of caspase-3 and PARP proteolytic cleavage after treatment with NXN-7, NXN-11, and nutlin-3 after 24 h. Total protein extracts from the samples with: lane 1: no treatment, 2: DMSO (1%), 3: nutlin-3 (10 μM), 4: NXN-7 (20 μM), 5: NXN-7 (40 μM), 6: NXN-11 (20 μM), and 7: NXN-11 (40 μM).

Modulation of p53-dependent gene expression

The p53 protein regulates the expression of multiple genes involved in the regulation of cell-cycle progression, apoptosis, and survival. One of the most critical gene targets of p53 in regard to cell-cycle control and apoptosis are $p21^{waf1/cip1}$ and members of Bcl2 protein family, PUMA and Noxa. Using RT-PCR we tested the expression of p21, PUMA, and Noxa in PA-1 cells treated with NXN-7, NXN-11, and the control compound nutlin-3. As shown in Figure 12, the expression of all three genes (by NXN-7) and PUMA and Noxa (by NXN-11) was up-regulated by NXN-7 and NXN-11 in PA-1 cells; however, the up-regulation of p21 by NXN-11 was still very low after 4 h and reached its maximum after 8 h (Figure 13). Although the level of induction of p21 RNA by nutlin-3 was significantly higher than with NXN-7 and NXN-11, we found that the concentrations of the other two p53-responsive genes tested (PUMA and Noxa) were similar in cells treated by all three compounds. The expression of p21, PUMA, and Noxa was also evaluated in time-course experiments in which PA-1 and PA-1/E6 cells were treated with compounds for 4, 8, 16, and 24 h. As shown in

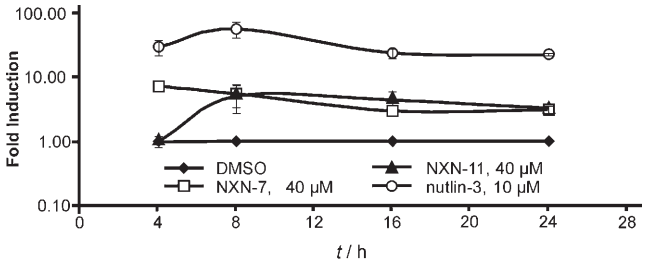

Figure 13. Time-dependent expression of p21 RNA in PA-1 cells treated with NXN compounds or nutlin-3.

Figure 13, the total level of p21 RNA in PA-1 cells treated with nutlin-3 at 10 μM during the period of time tested was strongly elevated and reached a maximum at 8 h after treatment. NXN-7 showed a slightly different pattern of p21 induction, with a maximum at 4 h and slow decrease during the course of the experiment.

NXN-11 produced very a similar p21 RNA induction profile as that of NXN-7, but with a maximum at 8 h and later. In contrast to NXN-7 and nutlin-3, NXN-11 showed only a very modest induction of p21 in PA-1 cells after 4 h incubation. In contrast to p21, the induction of PUMA expression in PA-1 cells by NXN-7 at 40 μM and nutlin-3 at 10 μM was almost the same, with NXN-11 following the pattern of the first two molecules with a slightly less significant effect after 4 h incubation (Figure 14).

In contrast to both NXN-7 and nutlin-3, NXN-11 was able to effect much stronger induction of Noxa RNA in PA-1 cells, especially after 4 h incubation (Figure 15). Even more importantly, neither of these reporter genes was induced by NXN-7 and

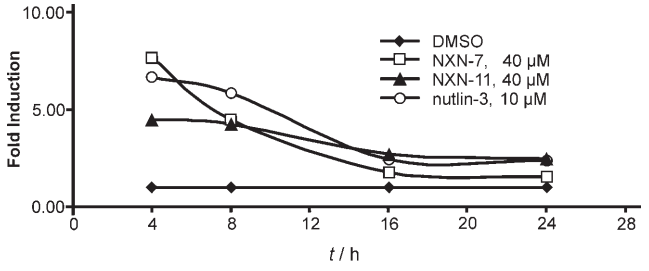

Figure 14. Time-dependent expression of PUMA RNA in PA-1 cells treated with NXN compounds or nutlin-3.

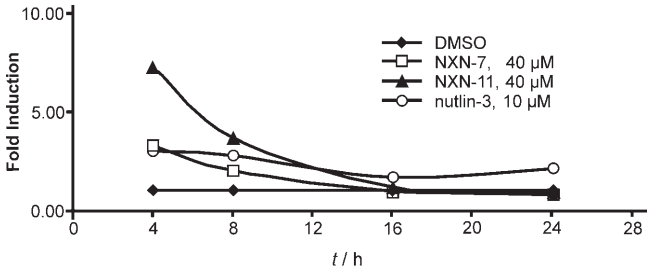

Figure 15. Time-dependent expression of Noxa RNA in PA-1 cells treated with NXN compounds or nutlin-3.

nutlin-3 in PA-1/E6 cells, which is consistent with absence of functional p53 protein in these cells (data not shown).

Similarly to NXN-7 and nutlin-3, NXN-11 was unable to elevate p21 and PUMA expression in PA-1/E6 cells. However, it did induce the same level of expression of Noxa in PA-1 and PA-1/E6 cells, pointing towards an alternative mechanism of action unrelated to disrupting the MDM2–p53 interaction.

To complement these RT-PCR studies, we purified protein extracts from PA-1 cells treated with NXN-7, NXN-11, and nutlin-3 after 4, 8, and 16 h incubation and verified the level of expression of p53 and p21 proteins. The stabilisation of p53 and induction of p21 proteins was strongest in the cells treated with nutlin-3 (Figure 16), and a dose- and time-dependent effect on

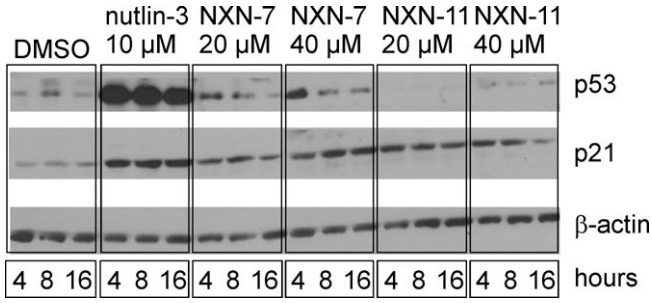

Figure 16. Time-dependent stabilisation of p53 and induction of p21 in PA-1 cells.

the level of expression of these proteins by NXN-7 was found as well. The best level of stabilisation of p53 and activation of p21 proteins was found in PA-1 cells treated with NXN-7 at 40 μM after 4 h incubation. Consistent with the RT-PCR results, induction of the p21 protein by NXN-11 was similar to NXN-7, whereas NXN-11 did not cause stabilisation of the p53 protein at any of the time points and concentrations tested. Therefore, the results of RT-PCR and Western blot experiments clearly suggest an alternative mechanism of action for NXN-11 versus NXN-7 and nutlin-3.

Conclusions

Herein we report the successful combination of straightforward in silico design and NMR-based methods to identify new small-molecule protein–protein interaction inhibitors that are potential lead molecules for a drug-discovery project. Based on physicochemical binding data, 2,3-substituted isoquinolin-1-one-4-carboxylic acid derivatives were identified that bind specifically to the MDM2 N-terminal domain p53 binding site without its denaturation. These compounds displace the p53 peptide from a preformed complex with MDM2 in vitro. With NMR and binding assays we demonstrated the competitive release of p53 from MDM2 and binding with fast on- and off-rate kinetics. Both NXN-6 and NXN-7 bind with K_D values in the low micromolar range. The released p53 is still folded, and the inhibitors do not induce precipitation or denaturation of MDM2. The compounds also show a differential activity towards p53 wild-type versus p53 knock-out cell lines, are able to induce specific genes downstream of p53, and induce early apoptosis.

The cellular activities of the second scaffold, NXN-11, are different from those of both nutlin-3 and NXN-7; NXN-11 does not stabilise p53 and induces late instead of early apoptosis. However, it did induce p21, PUMA, and Noxa expression. The NMR data gave an unambiguous explanation for the difference in the mode of action between NXN-7 and NXN-11 in cell lines. Because NXN-11 binds only weakly to MDM2 and is unable to dissociate the complex between MDM2 and p53 in vitro, we conclude that the cellular activity of NXN-11 is unrelated to the disruption of the MDM2–p53 interaction and results instead from binding to an unrelated and yet unknown target. Because of its biological properties, it may still be an interesting candidate for drug design once its target has been determined.

The 2,3-substituted isoquinolin-1-one-4-carboxylic acid derivatives provide a promising basis for the design of new derivates specific for the MDM2–p53 interaction. While the free carboxylic acid NXN-6 is not active on cell lines, the weakness of NXN-7 is its poor solubility. A follow-up compound (NXN-561) exhibited both improved solubility and cellular activity. Quite unexpectedly, it was found that both enantiomers of NXN-561 bind with approximately the same K_D value to MDM2.

Experimental Section

WST-1 proliferation assay: Proliferation in PA-1 and PA-1/E6 cell lines was measured 48 h after the addition of compounds to cells using WST-1 reagent (Roche Applied Sciences, Indianapolis, IN, USA) according to standard protocols. Survival curves were based on at least six concentration points, with values determined in at least three separate experiments, with each assay performed in sextuplicate. All statistical analyses were performed using the Excel-fit software program (ID Business Solutions, Bridgewater, NJ, USA). All experiments were repeated independently at least three times with six repeats of each data point.

Apoptosis annexin V and TUNEL assays: Annexin V and BrdU-incorporation levels were determined with Guava Nexin and Guava TUNEL kits using a Guava Personal Cell Analysis System (PCAS, Guava Technologies, Hayward, CA, USA) according to the manufacturer's instructions. PA-1 and PA-1/E6 cells ($\sim 1\times10^6$) were cultured in BME medium supplemented with 10% foetal bovine serum and various concentrations of inhibitors or DMSO for 24 h. Racemic nutlin-3 (Calbiochem, Roche) at 10 μM was applied as positive control. For the Guava Nexin assay, cells were trypsinised and collected by centrifugation at 1000 rpm with a Sorvall RT7 centrifuge, RTH-

250 rotor (600 *g*) for 5 min at 4 °C. After washing with ice-cold Nexin buffer (1×), cells were resuspended in the same buffer, labelled with annexin V-PE and 7-aminoactinomycin D in the dark on ice for 20 min, and then analysed with the PCAS. According to the manufacturer's protocol for the Guava TUNEL assay, cells were resuspended in 1% paraformaldehyde, incubated on ice for 60 min, and washed in ice-cold phosphate-buffered saline (PBS). Cells were then fixed in ice-cold 70% EtOH for at least 16 h at −20 °C. After incubation, cells were labelled with BrdU DNA labelling mix for 60 min at 37 °C and collected by centrifugation at 1000 rpm with a Sorvall RT7 centrifuge, RTH-250 rotor (600 *g*) for 5 min. Cells were resuspended in anti-BrdU staining mix and incubated at room temperature for 45 min in the dark, and then analysed with the PCAS.

Western blot: Whole-protein extracts (50 mg) from samples treated with NXN compounds, nutlin-3a or 1% DMSO were analysed by cleaved caspase-3 rabbit monoclonal antibody (Cell Signaling) and by mouse anti-PARP (poly(ADP-ribose) polymerase, BD Pharmingen) at respective dilutions of 1:1000 and 1:2000.

RT-PCR: Total RNA was extracted by using the RNeazy MiniKit (Qiagen, USA). cDNA was generated with GeneAmp:Gold RNA PCR Core Kit (Applied Biosystems, Foster City, CA) and amplified by semi-quantitative RT-PCR using Taq DNA polymerase (Qiagen, Canada) under the following conditions for RT-PCR: initial denaturation (94 °C, 3 min) and 25 cycles of denaturation (94 °C, 45 sec), annealing (50 °C, 45 sec), and extension (72 °C, 1 min). Primer sequences for $p21^{waf1/cip1}$: 5′-CCT CAT CCC GTG TTC TCC TTT-3′ and 5′-GTACCACCCAGCGGACAAGT-3′; for Noxa: 5′-GCG CAA GAA CGC TCA ACC-3′ and 5′-GCA AGT TTT TGA TGC AGT CAG G-3′; for PUMA: 5′-CCT GGA GGG TCC TGT ACA ATC T-3′ and 5′-GCA CCT AAT TGG GCT CCA TCT-3′.

Protein expression and purification: The recombinant human MDM2 (residues 1–118) was overexpressed at 37 °C in *E. coli* BL21-(DE3) using the pET46 vector (Novagen). The protein was renatured from *E. coli* inclusion bodies as previously described, and the refolded MDM2 was purified using a butyl Sepharose 4 Fast Flow column (Amersham).[20] The recombinant human GST-p53 protein (residues 1–73) was overexpressed at 37 °C in *E. coli* BL21 (DE3) using a pGEX vector. The protein was purified using a GST Sepharose Fast Flow column (Amersham). The final purification of all proteins was carried out with a HiLoad 16/60 Superdex 75 gel filtration column (Amersham).[11] The uniformly ^{15}N-enriched protein samples were prepared by growing the bacteria in minimal media containing $[^{15}N]NH_4Cl$.[20]

NMR spectroscopy: NMR spectra were acquired on a Bruker DRX 600 MHz spectrometer equipped with a cryoprobe and on a Bruker DRX 500 MHz instrument. Typically, NMR samples contained up to 0.2 mM protein in buffer at pH 7.4 containing 50 mM KH_2PO_4, 50 mM Na_2HPO_4, 150 mM NaCl, and 5 mM DTT. For the ^1H–^{15}N HSQC spectrum, a total of 2048 complex points in t_2 and 128 t_1 increments were acquired. Water suppression was carried out using the WATERGATE 5 sequence. NMR data were processed using the Bruker program Xwin-NMR version 3.5. Titration experiments were performed using a series of ^1H–^{15}N HSQC of labelled p53 or MDM2 along with the unlabelled partner. By monitoring the 1D ^1H NMR spectra, care was taken in preventing overtitration of the unlabelled sample.[11,12,20,21]

Ligand binding: Ligand binding experiments were carried out in an analogous way to that described previously.[20] Protein samples (500 μL) at a concentration of about 0.1 mM containing 10% D_2O, and a 20 mM stock solution of each compound in $[D_6]$DMSO were used in all of the experiments. Titrations were carried out with the inhibitors. The maximum concentration of DMSO at the end of titration experiments was about 2–3%. The pH was maintained constant during the entire titration.

ITC and Biacore experiments: The binding of various inhibitors to MDM2 (residues 1–118) was measured by isothermal titration calorimetry using a VP-ITC MicroCalorimeter (MicroCal, Northampton, MA, USA). The protein concentration in the reservoir solution was ~0.02–0.03 mM, and the concentration of the titrant was ~0.2–0.3 mM. Measurements were carried out in PBS with 2 mM TCEP, pH 7.4. All steps of the data analysis were performed using ORIGIN v. 5.0 software provided by the manufacturer.

***trans*-2-(4-Chlorobenzyl)-3-(4-chlorophenyl)-1-oxo-1,2,3,4-tetrahydroisoquinoline-4-carboxylic acid (NXN-6)**: 4-chlorobenzylamine (505.5 mg, 3.57 mmol) was added to a solution of 4-chlorobenzaldehyde (527 mg, 3.75 mmol) in 10 mL CH_2Cl_2 (peptide grade). The mixture was stirred in a round-bottom flask at room temperature for 1 h. Homophthalic acid (578.8 mg, 3.57 mmol) was then added, the reaction turned orange, and the mixture was stirred under reflux for 1 h. After cooling the mixture to room temperature, the formed precipitate was isolated by filtration and washed several times with CH_2Cl_2. The resulting white solid (1 g, 2.34 mmol) is a *cis*/*trans* mixture of the desired product in a 1:2 ratio. Afterwards, the isomeric mixture was treated with 40 mL acetic acid under reflux for 20 h. After evaporation of the solvent, the yellow residue was washed with 20 mL Et_2O to yield a white solid (750 mg, 75% yield); mp: 219.8–220.3 °C; ^1H NMR (250 MHz, DMSO): $\delta = 8.02$ (m, 2H), 7.49 (m, 2H), 7.30 (m, 6H), 7.21 (M, 1H), 7.05 (d, 2H, $J = 8.53$ Hz), 5.30 (s, 1H), 5.18 (d, 2H, $J = 15.01$ Hz), 4.11 (s, 1H), 3.96 ppm (d, 2H, $J = 15.01$ Hz); IR: $\tilde{\nu} = 2960$, 1698, 1643, 1490, 1466, 1399, 1306, 1288, 1257, 707 cm^{-1}; MS (−ESI): $m/z = 425$ [M−H]; Anal. calcd for $C_{23}H_{17}Cl_2NO_3$: C 64.80, H 4.02, N 3.29, found: C 64.59, H 4.10, N 2.96.

***trans*-2-(4-Chlorobenzyl)-3-(4-chlorophenyl)-1-oxo-1,2,3,4-tetrahydroisoquinoline-4-carboxylic acid (2-methoxyethyl)-amide (NXN-7)**: The coupling agent 1-ethyl-3-[3-(dimethylamino)propyl]-carbodiimide·HCl (EDCI, 881.8 mg, 4.6 mmol) was added to a solution of NXN-6 (1 g, 2.3 mmol) in 10 mL dry *N*,*N*-dimethylformamide (DMF). The mixture was stirred in a round-bottom flask at room temperature for 10 min. 2-Methoxyethylamine (345.5 mg, 4.6 mmol) was then added, and the mixture was stirred overnight at 50 °C. Afterwards, EtOAc (60 mL) was added, and the organic layer was washed two times with 40 mL brine, dried over $MgSO_4$, and the solvent was removed under vacuum. Finally, the crude product was purified by chromatography on silica gel with EtOAc/hexanes 4:1 as the eluent to afford the desired product as a white solid (333 mg, 30% yield); mp: 248.8–249.2 °C; ^1H NMR (250 MHz, DMSO): $\delta = 8.26$ (m, 1H), 7.49 (m, 2H), 7.22 (m, 6H), 7.07 (m, 1H), 6.98 (d, 2H, $J = 8.53$ Hz), 5.43 (s, 1H), 5.41 (m, 1H), 5.34 (d, 1H, $J = 14.69$ Hz), 3.83 (d, 1H, $J = 14.69$ Hz), 3.71 (s, 1H), 3.20 (m, 4H), 3.15 ppm (s, 3H); ^{13}C NMR (62.89 MHz, DMSO): $\delta = 169.49$, 163.58, 137.35, 135.18, 133.77, 133.47, 133.00, 132.11, 129.98, 129.29, 129.18, 129.03, 128.97, 128.85, 128.55, 127.55, 70.47, 61.61, 58.70, 53.56, 49.52, 39.72 ppm; IR: $\tilde{\nu} = 3335$, 3057, 2972, 2921, 1674, 1642, 1545, 1490, 1470, 1448, 1402, 1304, 1292, 1264, 1093, 1015, 707 cm^{-1}; MS (+ESI): $m/z = 484$ [M+H]; Anal. calcd for $C_{26}H_{24}Cl_2N_2O_3$: C 64.60, H 5.00, N 5.80, found: C 64.23, H 4.85, N 5.46.

1-(4-Chlorobenzyl)-5-(4-chlorophenyl)-3-hydroxy-4-phenyl-1,5-dihydropyrrol-2-one (NXN-11): For the synthesis of NXN-11, we employed the Doebner reaction, reported in 1887,[23] a multicomponent reaction (3-MCR) that uses anilines, aldehydes, and pyruvic

acid derivates to synthesise quinolines. The Doebner reaction was reinvestigated by Weber et al.,[24] who illustrated the possible formation of pyrrol-2-ones. A stoichiometric mixture of 4-chlorobenzaldehyde (140.5 mg, 1 mmol) and 4-chlorobenzylamine (141.6 mg, 1 mmol) in EtOH (2 mL) was stirred for 1 h at room temperature. 2-Oxo-3-phenylpropionic acid (164.1 mg, 1 mmol) was then added, and the mixture was stirred for 2 days. The formed precipitate was isolated by filtration and washed with cold EtOH to yield a white solid (240 mg, 58.5% yield); mp: 198.0–199.0 °C; ^{1}H NMR (250 MHz, [D$_6$]DMSO): $\delta = 7.57$ (d, 2H, $J = 8.69$ Hz), 7.45 (s, 1H), 7.39 (m, 4H), 7.25 (m, 4H), 7.14 (d, 3H, $J = 8.53$ Hz), 5.48 (s, 1H), 4.76 (d, 1H, $J = 15.64$ Hz), 3.76 ppm (d, 1H, $J = 15.64$ Hz); ^{13}C NMR (62.89 MHz, DMSO): $\delta = 166.97$, 144.54, 136.95, 136.76, 133.49, 132.49, 132.35, 130.55, 130.16, 129.55, 129.17, 128.87, 127.60, 121.90, 60.56, 43.63 ppm; IR: $\tilde{\nu} = 3166$, 1696, 1688, 1491, 1450, 143, 1383, 1308, 1292, 1206, 1086, 1014, 835, 765 cm^{-1}; MS (+ESI): $m/z = 411$ [M+H]; Anal. calcd for $C_{23}H_{17}Cl_2NO_2$: C 67.33, H 4.18, N 3.41, found: C 66.97, H 4.13, N 3.57.

6-Chloro-1*H*-indole-3-carbaldehyde: $POCl_3$ (1.8 mL) was added dropwise to DMF (5 mL) in a three-necked flask between 15 and 20 °C. A solution of 6-chloro-1*H*-indole (1 g, 6.6 mmol) in DMF (2 mL) was added dropwise between 20 and 30 °C. The reaction mixture was stirred for 45 min at 37 °C. Afterwards, the reaction mixture was poured into a mixture of 15 g ice in 10 mL H_2O under stirring. NaOH (3.4 g, 18 mL) was added between 20 and 30 °C. The resulting mixture was then held at reflux for 5 min. After cooling to room temperature, the precipitate was filtered off and washed with 10 mL cold H_2O. Crystallisation from EtOH yielded 6-chloro-1*H*-indole-3-carbaldehyde as a white solid (1.04 g, 88% yield).

***trans*-2-(4-Chlorobenzyl)-3-(6-chloro-1*H*-indol-3-yl)-1-oxo-1,2,3,4-tetrahydroisoquinoline-4-carboxylic acid**: 4-Chlorobenzylamine (0.376 g, 2.7 mmol) was added to a suspension of 6-chloro-1*H*-indole-3-carbaldehyde (0.5 g, 2.8 mmol) in 10 mL 1,2-dichloroethane. The mixture was stirred in a round-bottom flask at 60 °C for 3 h. Homophthalic acid (0.437 g, 2.7 mmol) was then added, the reaction mixture turned orange, and was stirred under reflux for 1 h. After cooling the mixture to room temperature, the precipitate formed was isolated by filtration and washed several times with 1,2-dichloroethane to give the product as a yellow solid (466 mg, 37% yield).

***trans*-2-(4-Chlorobenzyl)-3-(6-chloro-1*H*-indol-3-yl)-1-oxo-1,2,3,4-tetrahydroisoquinoline-4-carboxylic acid pentafluorophenyl ester**: Pentafluorophenol (0.552 g, 3 mmol) was added to a suspension of EDCI (0.287 g, 1.5 mmol) in 8 mL EtOAc at 0 °C. After 10 min, 2-(4-chlorobenzyl)-3-(6-chloro-1*H*-indol-3-yl)-1-oxo-1,2,3,4-tetrahydroisoquinoline-4-carboxylic acid (0.466 g, 1 mmol) was added at 0 °C, and the reaction mixture was stirred for 1 h at room temperature. After evaporation of the solvent, the crude product was purified by chromatography on silica gel with EtOAc/hexanes 1:2 as the eluent to yield the final ester as a white solid (543 mg, 86% yield).

***trans*-2-(4-Chlorobenzyl)-3-(6-chloro-1*H*-indol-3-yl)-1-oxo-1,2,3,4-tetrahydroisoquinoline-4-carboxylic acid (2-methoxyethyl)-amide (NXN-552)**: 2-Methoxyethylamine (0.015 g, 0.2 mmol) was added to a suspension of the pentafluorophenyl ester (0.124 g, 0.2 mmol) in 2 mL dry THF. The reaction mixture was stirred for 10 min at room temperature. Afterwards, 20 mL CH_2Cl_2 was added, and the organic layer was washed with sodium hydrogen carbonate (20 mL satd. aq.), dried over $MgSO_4$, and the solvent was removed in vacuo. Finally, the crude product was purified by chromatography on silica gel with the eluent EtOAc/hexanes 4:1 to afford the desired product NXN-552 as a white solid (89.2 mg, 85% yield); mp: 208.1–209.3 °C; ^{1}H NMR (250 MHz, CD_3CN): $\delta = 10.48$ (s, 1H), 8.08–8.11 (m, 1H), 7.51 (d, 1H, 8.63 Hz), 7.40–7.46 (m, 2H), 7.36 (d, 1H, 1.59 Hz), 7.24–7.30 (m, 4H), 7.09–7.12 (m, 1H), 7.03 (dd, 2H, 1.82 Hz, 8.40 Hz), 6.61 (d, 1H, 1.81 Hz), 5.39 (s, 1H), 5.28 (d, 1H, 15.21 Hz), 4.07 (s, 1H), 3.96 (d, 1H, 15.21 Hz), 3.14–3.21 (m, 2H), 3.19 (s, 3H), 2.79–2.85 ppm (m, 2H); MS (+ESI): $m/z = 523$ [M+H], Anal. calcd for $C_{28}H_{25}Cl_2N_3O_3$: C 64.37, H 4.82, N 8.04, found: C 64.02, H 4.77, N 8.28.

***trans*-2-(4-Chlorobenzyl)-3-(6-chloro-1*H*-indol-3-yl)-1-oxo-1,2,3,4-tetrahydroisoquinoline-4-carboxylic acid [2-(4-methylpiperazin-1-yl)-ethyl]-amide (NXN-561)**: 2-(4-Methylpiperazin-1-yl)-ethylamine (0.028 g, 0.2 mmol) was added to a suspension of the pentafluorophenyl ester (0.124 g, 0.2 mmol) in 2 mL dry THF. The reaction mixture was stirred for 10 min at room temperature. Afterwards, CH_2Cl_2 (20 mL) was added, and the organic layer was washed with sodium hydrogen carbonate (20 mL satd. aq.), dried over $MgSO_4$, and the solvent was removed in vacuo. Finally, the crude product was purified by chromatography on silica gel with the eluent EtOAc/MeOH 1:1 to afford the desired product NXN-561 as a white solid (80.4 mg, 68% yield); mp: 198.5–199.2 °C; ^{1}H NMR (250 MHz, CDCl3): $\delta = 8.48$ (s, 1H), 8.25–8.29 (m, 1H), 7.58 (d, 1H, 8.52 Hz), 7.44–7.49 (m, 2H), 7.30 (d, 1H, 1.58 Hz), 7.21 (s, 4H), 7.10 (dd, 1H, 8.52 Hz, 1.73 Hz), 7.03–7.06 (m, 1H), 6.61 (d, 1H, 1.90 Hz), 5.97 (t, 1H, 4.26 Hz), 5.76 (s, 1H), 5.34 (d, 1H, 14.69 Hz), 3.96 (s, 1H), 3.93 (d, 1H, 14.69 Hz), 3.00–3.16 (m, 2H), 2.17–2.23 (m, 10H), 2.20 ppm (s, 3H); IR: $\tilde{\nu} = 3268$, 2936, 2799, 1638, 1601, 1509, 1490, 1447, 1406, 1284, 1260, 1156, 1091, 1013, 798 cm^{-1}; MS (+ESI): $m/z = 591$ [M+H].

Separation of NXN-561 enantiomers (NXN-561a and NXN-561b): The preparative separation of racemic NXN-561 (180 mg) was performed using supercritical fluid chromatography (SFC) to receive pure (−)-NXN-561a (72.5 mg; $t_R = 1.34$ min, e.r. > 99.5:0.5, $[\alpha]_D^{20} = -15.5°$, $c = 0.94$ in MeOH) and (+)-NXN-561b (73.5 mg; $t_R = 2.16$ min, e.r. > 99.5:0.5, $[\alpha]_D^{20} = +15.1°$, $c = 0.96$ in MeOH) as colourless oils. Analytical and preparative SFC conditions: Berger SFCTM Minigram with a Chiralpak 5 μm, 4.6 mm × 250 mm AS-H (Daicel) column; isocratic 80% CO_2/20% MeOH + 0.5% Et_2NH as eluent; flow rate = 7 mL min^{-1}; outlet pressure = 1×10^4 kPa; column temperature = 35 °C; detection at $\lambda = 250$ nm. The material was injected as 100-μL stacked injections of a 10 mg mL^{-1} MeOH solution. Optical rotation values were measured with a PerkinElmer polarimeter 241.

Acknowledgements

We are grateful to Dr. Emde (Merck KGaA Darmstadt), who performed the separation of the NXN-561 enantiomers.

Keywords: compound design · MDM2 · NMR screening · p53 · protein–protein interactions

[1] D. P. Lane, *Nature* **1992**, *358*, 15–16.
[2] a) B. Vogelstein, D. Lane, A. J. Levine, *Nature* **2000**, *408*, 307–310; b) K. H. Vousden, X. Lu X, *Nat. Rev. Cancer* **2002**, *2*, 594–604.
[3] a) J. D. Oliner, K. W. Kinzler, P. S. Meltzer, D. L. George, B. Vogelstein, *Nature* **1992**, *358*, 80–83; b) X. Wu, J. H. Bayle, D. Olson, A. J. Levine, *Genes Dev.* **1993**, *7*, 1126–1132; c) S. M. Picksley, D. P. Lane, *Bioassays* **1993**, *15*, 689–690; d) J. Momand, G. P. Zambetti, D. C. Olson, D. George, A. J. Levine, *Cell* **1992**, *69*, 1237–1245; e) I. Ringshausen, C. C. O'Shea, A. J. Finch, L. B. Swigart, G. I. Evan, *Cancer Cell* **2006**, *10*, 501–514.

[4] D. Michael, M. Oren, *Cancer Biol.* **2003**, *13*, 49–58.
[5] a) J. Momand, D. Jung, S. Wilczynski, J. Niland, *Nucleic Acids Res.* **1998**, *26*, 3453–3459; b) D. A. Freedman, L. Wu, A. J. Levine, *Cell. Mol. Life Sci.* **1999**, *55*, 96–107.
[6] a) J. Chen, V. Marechal, A. J. Levine, *Mol. Cell. Biol.* **1993**, *13*, 4107–4114; b) C. Wasylyk, R. Salvi, M. Argentini, C. Dureuil, I. Delumeau, J. Abecassis, L. Debussche, B. Wasylyk, *Oncogene* **1999**, *18*, 1921–1934; c) G. Tortora, R. Caputo, V. Damiano, R. Bianco, J. Chen, S. Agrawal, A. R. Bianco, F. Ciardiello, *Int. J. Cancer* **2000**, *88*, 804–809; d) Z. Zhang, M. Li, H. Wang, S. Agrawal, R. Zhang, *Proc. Natl. Acad. Sci. USA* **2003**, *100*, 11636–11641.
[7] a) A. Böttger, V. Böttger, A. Sparks, W. L. Liu, S. F. Howard, D. P. Lane, *Curr. Biol.* **1997**, *7*, 860–869; b) D. P. Lane, *Br. J. Cancer* **1999**, *80 (Suppl 1)*, 1–5; c) P. Chène, *Nat. Rev. Cancer* **2003**, *3*, 102–109; d) P. Chène, *Cell Cycle* **2004**, *3*, 460–461.
[8] a) L. T. Vassilev, B. T. Vu, B. Graves, D. Carvajal, F. Podlaski, Z. Filipovic, N. Kong, U. Kammlott, C. Lukacs, C. Klein, N. Fotouhi, E. A. Liu, *Science* **2004**, *303*, 844–848; b) B. L. Grasberger, T. Lu, C. Schubert, D. J. Parks, T. E. Carver, H. K. Koblish, M. D. Cummings, L. V. LaFrance, K. L. Milkiewicz, R. R. Calvo, D. Maguire, J. Lattanze, C. F. Franks, S. Zhao, K. Ramachandren, G. R. Bylebyl, M. Zhang, C. L. Manthey, E. C. Petrella, M. W. Pantoliano, I. C. Deckman, J. C. Spurlino, A. C. Maroney, B. E. Tomczuk, C. J. Molloy, R. F. Bone, *J. Med. Chem.* **2005**, *48*, 909–912; c) J. Deng, R. Dayam, N. Neamati, *Expert Opin. Ther. Pat.* **2006**, *16*, 165–188.
[9] M. R. Arkin, J. A. Wells, *Nat. Rev. Drug Discovery* **2004**, *3*, 301–317.
[10] a) M. Krajewski, P. Ozdowy, L. D'Silva, U. Rothweiler, T. A. Holak, *Nat. Med.* **2005**, *11*, 1135–1136; b) Y. Lu, Z. Nikolovska-Coleska, X. Fang, W. Gao, S. Shangary, S. Qiu, D. Qin, S. Wang, *J. Med. Chem.* **2006**, *49*, 3759–3762.
[11] L. D'Silva, P. Ozdowy, M. Krajewski, U. Rothweiler, M. Singh, T. A. Holak, *J. Am. Chem. Soc.* **2005**, *127*, 13220–132206.
[12] M. Krajewski, U. Rothweiler, S. Majumdar, L. D'Silva, C. Klein, T. A. Holak, *J. Med. Chem.* **2007**, *50*, 4382–4387.
[13] R. Nilakantan, N. Bauman, J. S. Dixon, R. Venkataraghavan, *J. Chem. Inf. Comput. Sci.* **1987**, *27*, 82–85.
[14] R. P. Sheridan, J. Shpungin, *J. Chem. Inf. Comput. Sci.* **2004**, *44*, 727–740.
[15] Program toto2 simsearch, OntoChem GmbH, http://www.ontochem.-com.
[16] B. Huang, M. Schroeder, *BMC Struct. Biol.* **2006**, *6*, 19.
[17] Gerber Molecular Design, http://www.moloc.ch.
[18] a) M. Cushman, J. Gentry, F. W. Dekow, *J. Org. Chem.* **1977**, *42*, 1111–1116; b) M. Cushman, T. C. Choong, J. T. Valko, M. P. Koleck, *J. Org. Chem.* **1980**, *45*, 5067–5073; c) L. Wang, J. Liu, H. Tian, C. Qian, J. Sun, *Adv. Synth. Catal.* **2005**, *347*, 689–694; d) N. Yu, L. Bourel, B. Deprez, J. C. Gesquiere, *Tetrahedron Lett.* **1998**, *39*, 829; e) J. S. Yadav, B. V. S. Reddy, S. S. Raj, R. A. Prasad, *Tetrahedron* **2003**, *59*, 1805–1809.
[19] M. P. Stoyanova, S. E. Angelova, K. S. Kosev, P. S. Denkova, V. G. Enchev M. D. Palamareva, *Tetrahedron Lett.* **2006**, *47*, 2119–2123.
[20] R. Stoll, C. Renner, S. Hansen, S. Palme, C. Klein, A. Belling, W. Zeslawski, M. Kamionka, T. Rehm, P. Muhlhahn, *Biochemistry* **2001**, *40*, 336–344.
[21] G. M. Popowicz, A. Czarna, U. Rothweiler, A. Szwagierczak, M. Krajewski, L. Weber, T. A. Holak, *Cell Cycle* **2007**, *6*, 2386–2392.
[22] N. A. Laurie, S.L Donovan, C. S. Shih, J. Zhang, N. Mills, C. Fuller, A. Teunisse, S. Lam, Y. Ramos, A. Mohan, D. Johnson, M. Wilson, C. Rodriguez-Galindo, M Quarto, S. Francoz, S. M. Mendrysa, R. K. Guy, J. C. Marine, A. G. Jochemsen, M. A. Dyer, *Nature* **2006**, *444*, 61–66.
[23] a) O. Doebner, *Justus Liebigs Ann. Chem.* **1887**, *242*, 265; b) O. Doebner, *Ber. Dtsch. Chem. Ges.* **1887**, *20*, 277; c) O. Doebner, *Ber. Dtsch. Chem. Ges.* **1894**, *27*, 352.
[24] L. Weber, K. Illgen, M. Almstetter, *Synlett* **1999**, 366–374.

Received: January 30, 2008
Revised: March 26, 2008
Published online on April 21, 2008

